Supporting Information

A new type of Lanthanide−sodium metalloring organic framework featuring high proton conduction in a wide temperature range and detection of Fe3+ ions

Lizhen Liu,*[a] Gaoyong Zhu,[a] Kang Yang,[a] Yaozong Chen,[a] Yuan Hong,[b] Yiyang Bo,[a] Susu Wu,[a] Xiangfang Peng,*[a] and Zizhu Yao*[b]

a. Key Laboratory of Polymer Materials and Products of Universities in Fujian, Department of Materials Science and Engineering, Fujian University of Technology, Fuzhou 350118, P. R. China;

E-mail: liulizhen@fjut.edu.cn; pengxf@fjut.edu.cn;

b. Fujian Provincial Key Laboratory of Polymer Materials, College of Chemistry and Materials Science, Fujian Normal University, Fuzhou 350007, P. R. China;

E-mail: yaozizhu@fjnu.edu.cn;

1. Experimental

1.1 Materials and characterization methods

All reagents and solvents used in synthetic studies are commercially available and were used as supplied without further purification. Powder X-ray diffraction (PXRD) was carried out with a PANalytical X'Pert^3 powder diffractometer equipped with a Cu sealed tube (λ = 1.541874 Å) at 40 kV and 40 mA over the 2θ range of 5-30^o. The simulated pattern was produced using the Mercury V1.4 program and single-crystal diffraction data. Elemental analyses (C, H, S and N) were performed on a Perkin-Elmer 240C analyzer. FT-IR spectra of the synthesized complexes were carried out on a Nicolet 5700 FT-IR spectrometer as KBr pellets. Thermal analysis was carried out on a METTLER TGA/SDTA 851 thermal analyzer from 30 to 600 ^{o}C at a heating rate of 10 ^{o}C min^{-1} under N_2 flow. Excitation and emission spectra of the samples were recorded on Edinburgh FL980 spectrophotometer. X-ray photoelectron spectroscopy (XPS) was performed on the Thermo Scientific ESCALab 250Xi using 200 W monochromated Al Kα radiation. The 500 μm X-ray spot was used for XPS analysis. Typically the hydrocarbon C1s line at 284.8 eV from adventitious carbon is used for energy referencing. UV-visible study was performed with a Shimadzu spectrophotometer (UV-2600i).

1.2 Synthesis and characterization of $\{[(Me_2NH_2)_{1.25}(H_3O)_{4.25}Na_{1.5}Eu_2(\mu_2\text{-}OH)(H_2O)(SIP)_4]\bullet(DMA)\cdot 7.5H_2O\cdot 0.5CH_3OH\}_n$ (**FUT-2-Eu**)

NaH_2SIP (0.134 g, 0.05 mmol) and $Eu(NO_3)_3$ (0.044g, 0.1 mmol) were dissolved in mixed solution of DMA (4 mL),H_2O (2 mL), and CH_3OH (4 mL). The above mixture was transferred into a Teflon-lined stainless steel autoclave (20 mL) and heated at 120 ^{o}C for 48 h. After being cooling to room temperature slowly, the colorless block crystals of **FUT-2-Eu** were obtained and washed with fresh DMA (yield: 36% based on NaH_2SIP). IR (KBr, cm^{-1}): 3436 (s), 3423 (s, br), 1609 (s), 1551 (s), 1450 (s), 1388 (s), 1174 (m), 1048 (s), 782 (w), 721 (s), 675 (w), 627 (s), 583 (w). Elemental analysis calcd (%) for $C_{39}H_{63.75}N_{2.25}O_{43.25}Na_{1.5}S_4Eu_2$: C, 27.19; H, 3.73; N, 1.83; S, 7.44; Found: C,27.91; H, 3.68; N, 1.83; S,7.10.

1.3 Synthesis and characterization of $\{[(Me_2NH_2)_{1.25}(H_3O)_{4.25}Na_{1.5}Sm_2(\mu_2\text{-}OH)(H_2O)(SIP)_4]\bullet 0.7(DMA)\cdot 5.5H_2O\cdot 3CH_3OH\}_n$ (**FUT-2-Sm**)

NaH_2SIP (0.268 g, 1 mmol) and $Sm(NO_3)_3$ (0.065g, 0.2 mmol) were dissolved in mixed solution of DMA (4 mL), H_2O (2 mL), and CH_3OH (4 mL). The above mixture was transferred into a Teflon-lined stainless steel autoclave (20 mL) and heated at 120 ^oC for 24 h. After being cooling to room temperature slowly, the colorless block crystals of **FUT-2-Sm** were obtained and washed with fresh DMA (yield: 30% based on NaH_2SIP). IR (KBr, cm^{-1}): 3737 (s), 3399 (s, br), 1609 (s), 1548 (s), 1442 (m), 1375 (s), 1182 (s), 1103 (m), 1048 (s), 885 (w), 781 (m), 724 (s), 681 (w), 627 (s), 525 (w). Elemental analysis calcd (%) for $C_{40.3}H_{67.05}N_{1.95}O_{43.45}Na_{1.5}S_4Sm_2$: C, 27,86; H, 3.89; N, 1.57; S, 7.38; Found: C,28.09; H, 3.74; N, 1.57; S,7.04.

1.4 Single-crystal X-ray diffraction

Data collection and structural analysis of **FUT-2-Eu** and **FUT-2-Sm** were performed on an Agilent Technologies SuperNova single crystal diffractometer equipped with graphite monochromatic Cu Ka radiation (λ = 1.54184Å). The crystal was kept at 150K and 299 K and during data collection, respectively. Using Olex2[1], the structure was solved with the Superflip[2] structure solution program using charge flipping and refined with the ShelXL[3] refinement package using least squares minimization. All nonhydrogen atoms were refined with anisotropic displacement parameters. The hydrogen atoms on the ligands were placed at idealized positions and refined using a riding model. We employed PLATON[4] and SQUEEZE[5] to calculate the diffraction contribution of the solvent molecules and thereby produce a set of solvent-free diffraction intensities. The detailed crystallographic data and structure refinement parameters for these compounds are summarized in Table S2-S3 (CCDC: 2340669-2340670)

1.5 Proton conductivity measurement

The alternating-current (AC) impedance measurement procedure was similar to our perviously reported[6-7]. Firstly, the as-synthesized sample was finely ground to a powder and compressed into a homemade cylindrical closed glass container with an inner diameter of 0.4 cm. The sample thickness of 3.67 and 4.16 cm, respectively, for

FUT-2-Eu and **FUT-2-Sm** was measured using a vernier caliper. AC impedance measurements were carried out using a two-probe method with stainless steel-pressed electrodes in a Solartron SI 1260 Impedance/Gain-Phase Analyzer and 1296 Dielectric Interface Impedance Analyzer over the frequency range of 100 Hz to 1 MHz and the temperature range from subzero to 90 ^{o}C with an input voltage of 100 mV. Measurements were performed at thermal equilibrium by holding for 30 minutes at each measuring temperature. Proton conductivity was calculated using the following equation:

$$\sigma = \frac{l}{SR} \qquad (1)$$

Where l and S are the length (cm) and cross-sectional area (cm^2) of the samples, respectively, and R, which was extracted directly from the impedance plots, is the bulk resistance of the sample (Ω). Activation energy (E_a) for the material conductivity was estimated from the following equation:

$$\sigma T = \sigma_0 \exp(-\frac{E_a}{k_B T}) \qquad (2)$$

Where σ is the proton conductivity, σ_0 is the preexponential factor, k_B is the Boltzmann constant, and T is the temperature.

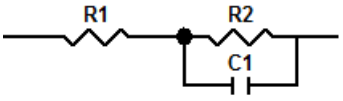

(3)

ZView software was used to extrapolate impedance data results by means of an equivalent circuit simulation (3) to complete the Nyquist plot and obtain the resistance values.

1.6 Luminescent measurements

The well-ground **FUT-2-Eu** (10 mg) samples were separately soaked in 5 mL of 1×10^{-3} mol/L $M(NO_3)_x$ (M = Al^{3+}, Cd^{2+}, Co^{2+}, Cu^{2+}, K^+, Mn^{2+}, Na^+, Ni^{2+}, Zn^{2+}, Fe^{3+}) DMA solutions and ultrasonicated for 3 h to form a stable and uniformly dispersed suspension. The corresponding fluorescence emission spectra recorded by Edinburgh FL980 spectrophotometer. The strongest emission wavelengths for **FUT-2-**

Eu were located at 616 nm when excited at 299 nm. The luminescence decay experiments (lifetimes) were performed on an Edinburgh Analytical instrument FLS1000 equipped with an OPO laser. The absolute PL quantum yields of power samples were measured by FLS1000 equipped with an integrating sphere.

Detection limit of Fe^{3+} was determined according to the following definitions:

$$\delta = \sqrt{\frac{\sum_{i=1}^{n}\left(x_i - \bar{x}\right)^2}{n-1}} \quad \textbf{(1)}$$

$$k = \frac{\Delta I}{\Delta C} \quad \textbf{(2)}$$

$$DL = \frac{3\delta}{k} \quad \textbf{(3)}$$

Where δ is the standard deviation of 10 replicated emission intensities for the blank sample; where △I and △c represent the variation of the luminescence intensity and the concentration before and after adding Fe^{3+}, respectively, the value of slope k was calculated. Finally the detection limit, DL, was calculated according to Function 3.

1.7 Grand Canonical Monte Carlo (GCMC) Simulations

The charges of **FUT-2-Eu** was determined by the population analysis using the Qeq in MaterialsStudio (Accelrys, Materials Studio Getting Started, release 5.0, Accelrys Software, Inc, San Diego, CA, 2009) [8]. The GCMC simulations were performed using the Materials Studio' Sorption modules to calculate the energy distribution and density distribution of Fe^{3+} adsorbed on the **FUT-2-Eu**. A 2×2×2 crystallographic unit cell was used for GCMC simulation. The rigid framework assumption was used in all simulations.

In addition, the simulations were also carried out at 296 K, adopting the locate task. Metropolis method in Sorption module and the universal forcefield (UFF). The cutoff radius was chosen as 18.5 Å for the LJ potential and the long-range electrostatic

interactions were handled using the Ewald summation method. The loading steps and the equilibration steps were 1×10^6, the production steps were 1×10^7.

Table S1 Crystal data and refinement results for the as-synthesized samples.

Identification code	**FUT-2-Eu**	**FUT-2-Sm**
Empirical formula	$C_{39}H_{63.75}N_{2.25}O_{43.25}Na_{1.5}S_4Eu_2$	$C_{40.3}H_{67.05}N_{1.95}O_{43.45}Na_{1.5}S_4Sm_2$
Formula weight	1722.84	1737.56
Temperature/K	150.00(10)	299.58(10)
Crystal system	monoclinic	monoclinic
Space group	*C2/c*	*C2/c*
a/Å	24.1324(3)	24.1627(12)
b/Å	27.9543(5)	28.0873(12)
c/Å	22.9415(4)	22.9131(7)
α/°	90	90
β/°	97.7240(10)	98.693(4)
γ/°	90	90
V/Å^3	15336.0(4)	15371.7(11)
Z	8	8
ρ_{calc}g/cm^3	1.179	1.167
μ/mm^{-1}	13.245	12.998
F(000)	5284.0	5244.0
Radiation	Cu Kα (λ = 1.54184)	Cu Kα (λ = 1.54184)
Data/restraints/parameters	13532/325/669	13708/372/690
Goodness-of-fit on F^2	1.098	1.082
Final R indexes [I>=2σ	R_1 = 0.0859,	R_1 = 0.0863,
(I)][a]	wR_2 = 0.2376	wR_2 = 0.2382
Final R indexes [all data][a]	R_1 = 0.1016,	R_1 = 0.0990,
	wR_2 = 0.2542	wR_2 = 0.2496

[a]$R_1 = \sum(|F_o| - |F_c|) / \sum|F_o|$, [b]$wR_2 = [\sum w(F_o^2 - F_c^2)^2 / \sum w(F_o^2)^2]^{0.5}$

Table S2 Selected bond lengths and bond angle for **FUT-2-Eu**.

Atom-Atom	Length/Å	Atom-Atom	Length/Å
Eu1-O20[1]	2.610(6)	Eu1-O4[2]	2.512(6)
Eu1-O1	2.297(6)	Eu1-O22[3]	2.690(6)
Eu1-O3[2]	2.465(6)	Eu1-O23[3]	2.472(6)
Eu1-O8	2.345(7)	Eu1-O19[1]	2.438(6)
Eu1-O14[3]	2.334(7)	Eu2-O31[3]	2.345(6)
Eu2-O16	2.570(6)	Eu2-O22	2.442(7)
Eu2-O15	2.407(7)	Eu2-O27[1]	2.472(7)
Eu2-O13	2.333(7)	Eu2-O28[1]	2.445(6)
Eu2-O23	2.325(6)	O31-Eu2[3]	2.345(6)
O31-Na2	2.412(6)	O12-Na1[3]	2.374(7)
O12 -Na2	2.513(7)	O16-Na2[3]	2.770(6)
O20-Eu1[1]	2.610(6)	O20-Na1[1]	2.536(7)
O4-Eu1[2]	2.512(6)	O22-Eu1[3]	2.690(6)
O3- Eu1[2]	2.465(6)	O23-Eu1[3]	2.472(6)
O27-Eu2[1]	2.472(7)	O28-Eu2[1]	2.445(6)
O28-Eu2[1]	2.520(7)	O10-Na1	O10 Na1
O19-Eu1[1]	2.438(6)	O14-Eu1[3]	2.334(7)
Na1-O12[3]	2.374(7)	Na1-O20[1]	2.536(7)
Na1-O21	2.393(7)	Na1-O21[1]	2.438(7)
Na1-O10W	2.430(9)	Na2-O31[5]	2.412(6)
Na2-O12[5]	2.513(7)	Na2-O16[3]	2.770(6)
Na2-O16[4]	2.770(6)	Na2-O28[3]	2.520(7)
Na2-O28[4]	2.520(7)	O21-Na1[1]	2.438(7)
O2-Eu2[3]	2.325(6)		
Atom-Atom-Atom	**Angle/°**	**Atom-Atom-Atom**	**Angle/°**
O20[1]-Eu1-O22[2]	133.48(19)	O1-Eu1-O20[1]	128.0(2)
O1-Eu1- O4[3]	71.5(2)	O1- Eu1-O22[2]	73.5(2)
O1-Eu1-O33	124.1(2)	O1- Eu1-O23[2]	83.9(3)
O1- Eu1-O8	148.6(2)	O1- Eu1-O19[1]	80.1(2)
O1- Eu1-O14[2]	83.3(3)	O4[3] -Eu1-O20[1]	108.5(2)
O4[3] -Eu1-O22[2]	117.85(19)	O3[3]-Eu1-O20[1]	73.1(2)
O3[3] -Eu1-O4[3]	52.8(2)	O3[3]-Eu1-O22[2]	134.0(2)
O3[3] -Eu1-O23[2]	86.8(2)	O23[2]-Eu1-O20[1]	147.9(2)
O23[2]-Eu1-O4[3]	76.1(2)	O23[2]-Eu1-O22[2]	50.4(2)
O8-Eu1-O20[1]	77.7(2)	O8-Eu1-O4[3]	121.8(2)
O8-Eu1-O22[2]	75.2(2)	O8-Eu1-O3[3]	77.0(2)
O8-Eu1-O23[2]	73.5(3)	O8-Eu1-O191	129.0(2)
O19[1]-Eu1-O20[1]	51.7(2)	O19[1]-Eu1-O4[3]	76.2(2)
O19[1]-Eu1-O22[2]	142.9(2)	O19[1]-Eu1-O3[3]	82.6(2)
O19[1]-Eu1-O23[2]	151.2(2)	O142-Eu1-O20[1]	72.5(2)
O14[2]-Eu1-O4[3]	148.6(2)	O14[2]-Eu1-O22[2]	70.2(2)
O14[2]-Eu1-O3[3]	144.9(2)	O14[2]-Eu1-O23[2]	120.5(2)

O14^{2}-Eu1-O8	89.5(2)	O14^{2}-Eu1-O19^{1}	81.3(3)
O31^{2}-Eu2-O16	74.7(2)	O31^{2}-Eu2-O22	78.8(2)
O31^{2}-Eu2 -O15	127.3(2)	O31^{2}-Eu2-O27^{1}	114.9(2)
O31^{2}-Eu2-O28^{1}	77.1(2)	O22-Eu2-O16	153.5(2)
O22-Eu2- O27^{1}	76.9(2)	O22-Eu2-O28^{1}	103.8(2)
O15-Eu2- O16	52.7(2)	O15-Eu2-O22	153.8(2)
O15-Eu2- O27^{1}	88.0(3)	O15-Eu2-O28^{1}	82.7(2)
O 27^{1}-Eu2-O16	115.4(2)	O13-Eu2-O31^{2}	80.8(2)
O13-Eu2- O16	80.0(2)	O13-Eu2-O22	94.9(2)
O13-Eu2- O15	92.2(3)	O13-Eu2-O27^{1}	159.8(2)
O13-Eu2- O28^{1}	147.5(2)	O28^{1}-Eu2-O16	71.4(2)
O28^{1}-Eu2-O27^{1}	52.5(2)	O22-Eu2-O31^{2}	155.7(2)
O22-Eu2- O16	121.7(2)	O22-Eu2-O22	83.2(2)
O22-Eu2- O15	72.3(2)	O22-Eu2-O27^{1}	76.1(2)
O22-Eu2- O13	84.7(2)	O22-Eu2-O28^{1}	123.4(2)
O12^{2}-Na1-O20^{1}	95.4(2)	O12^{2}-Na1-O21	86.4(2)
O12^{2}-Na1-O21^{1}	82.5(2)	O12^{2}-Na1-O10W	167.1(3)
O10-Na1-O12^{2}	107.2(2)	O10-Na1-O20^{1}	93.2(2)
O10-Na1-O21^{1}	80.6(3)	O10-Na1-O21	155.4(3)
O10-Na1-O10W	84.9(3)	O21^{1}-Na1-O20^{1}	172.5(2)
O21-Na1-O20^{1}	106.2(2)	O21-Na1-O21^{1}	80.9(2)
O21-Na1-O10W	84.0(3)	O10W-Na1-O20^{1}	79.3(3)
O10W-Na1-O21^{1}	104.3(3)	O31-Na2-O31^{5}	156.0(4)
O31-Na2-O12	53.81(18)	O31-Na2-O12^{5}	145.9(2)
O31^{5}-Na2-O12^{5}	53.81(19)	O31^{5}-Na2-O12	145.9(2)
O31^{5}-Na2-O16^{2}	116.61(19)	O31^{5}-Na2-O16^{4}	70.01(19)
O3^{1}- Na2-O16^{2}	70.01(19)	O31-Na2-O16^{4}	116.61(19)
O3^{1}- Na2-O28^{4}	74.5(2)	O31-Na2-O28^{2}	86.8(2)
O31^{5}-Na2-O28^{4}	86.8(2)	O31^{5}-Na2-O28^{2}	74.5(2)
O12^{5}-Na2-O12	110.5(3)	O12-Na2-O16^{2}	84.4(2)
O12-Na2-O16^{4}	78.91(19)	O12^{5}-Na2-O16^{4}	84.4(2)
O12^{5}-Na2-O16^{2}	78.91(19)	O12-Na2-O28^{4}	127.2(2)
O12-Na2-O28^{2}	106.3(2)	O12^{5}-Na2-O28^{4}	106.3(2)
O12^{5}-Na2-O28^{2}	127.2(2)	O28^{4}-Na2-O16^{2}	67.0(2)
O28^{2}-Na2-O16^{2}	141.9(3)	O28^{2}-Na2-O16^{4}	67.0(2)
O28^{4}-Na2-O16^{4}	141.9(3)	O28^{2}-Na2-O28^{4}	78.0(4)

^{1}1-X,+Y,1/2-Z; ^{2}1-X,1-Y,1-Z; ^{3}3/2-X,1/2-Y,1-Z; ^{4}+X,1-Y,1/2+Z; ^{5}1-X,+Y,3/2-Z

Table S3 Selected bond lengths and bond angle for **FUT-2-Sm**.

Atom-Atom	Length/Å	Atom-Atom	Length/Å
Sm1-O22	2.327(8)	Sm1-O4^{1}	2.372(6)
Sm1-O15	2.583(6)	Sm1-O28^{2}	2.471(6)
Sm1-O26	2.474(7)	Sm1-O27	2.460(6)
Sm1-O14	2.416(8)	Sm1-O6	2.368(7)
Sm2-O13^{3}	2.635(7)	Sm2-O20^{4}	2.516(7)
Sm2-O19^{4}	2.501(8)	Sm2-O28^{2}	2.688(6)
Sm2-O29^{2}	2.499(7)	Sm2-O21	2.328(9)
Sm2-O21	2.371(8)	Sm2-O12^{3}	2.428(8)
Sm2-O7	2.371(7)	Na2-O4^{5}	2.416(6)
Na2-O4	2.416(6)	Na2-O15^{3}	2.812(8)
Na2-O15^{1}	2.812(8)	Na2-O5	2.525(7)
Na2-O5^{5}	2.525(7)	Na2-O27^{3}	2.508(8)
Na2-O27^{1}	2.508(8)	Na1-O13^{3}	2.505(8)
Na1-O5	2.360(8)	Na1-O8	2.413(8)
Na1-O8^{5}	2.464(9)	Na1-O1^{1}	2.437(11)
Na1-O1W	2.419(10)	O4-Sm1^{1}	2.372(6)
O13-Sm2^{6}	2.635(7)	O13-Na1^{6}	2.505(8)
O15-Na2^{1}	2.812(8)	O20-Sm2^{4}	2.516(7)
O19-Sm2^{4}	2.501(8)	O28-Sm1^{2}	2.471(6)
O28-Sm2^{2}	2.688(6)	O29-Sm2^{2}	2.499(7)
O8-Na1^{5}	2.464(9)	O27-Na2^{1}	2.508(8)
O2-Sm2^{1}	2.371(8)	O1-Na1^{1}	2.437(11)
O12-Sm2^{6}	2.428(8)		

Atom-Atom-Atom	Angle/°	Atom-Atom-Atom	Angle/°
O22-Sm1-O15	122.9(3)	O22-Sm1-O28^{2}	82.7(3)
O22-Sm1-O4^{1}	155.3(2)	O22-Sm1-O26	76.3(3)
O22-Sm1-O27	123.6(3)	O22-Sm1-O14	72.8(3)
O22-Sm1-O6	85.2(3)	O4^{1}-Sm1-O15	74.6(2)
O41-Sm1-O28^{2}	79.0(2)	O4^{1}-Sm1-O26	115.0(2)
O4^{1}-Sm1-O27	77.2(2)	O4^{1}-Sm1-O14	126.9(2)
O28^{2}-Sm1-O15	153.6(2)	O28^{2}-Sm1-O26	77.2(2)
O26-Sm1-O15	115.4(2)	O27-Sm1-O15	71.6(2)
O27-Sm1-O28^{2}	104.0(2)	O27-Sm1-O26	52.3(2)
O14-Sm1-O15	52.3(2)	O14-Sm1-O28^{2}	154.1(2)
O14-Sm1-O26	88.7(3)	O14-Sm1-O27	83.3(3)
O6-Sm1-O4^{1}	80.1(3)	O6-Sm1-O15	79.1(2)
O6-Sm1-O28^{2}	95.1(2)	O6-Sm1-O26	160.7(3)
O6-Sm1-O27	146.7(3)	O6-Sm1-O14	91.2(3)
O13^{3}-Sm2-O28^{2}	135.0(2)	O20^{4}-Sm2-O13^{3}	107.1(3)
O20^{4}-Sm2-O28^{2}	117.7(2)	O19^{4}-Sm2-O13^{3}	72.8(3)
O19^{4}-Sm2-O20^{4}	52.5(3)	O19^{4}-Sm2-O28^{2}	133.5(3)
O29^{2}-Sm2-O13^{3}	148.1(3)	O29^{2}-Sm2-O20^{4}	77.2(3)

O29[2]-Sm2-O19[4]	87.0(3)	O29[2]-Sm2-O28[2]	49.4(2)
O21-Sm2-O13[3]	127.7(3)	O21-Sm2-O20[4]	72.1(3)
O21-Sm2-O19[4]	124.4(3)	O21-Sm2-O28[2]	72.9(3)
O21-Sm2-O29[2]	84.0(3)	O21-Sm2-O21	149.3(3)
O21-Sm2-O12[3]	80.2(3)	O21-Sm2-O7	83.4(3)
O21-Sm2-O13[3]	77.5(3)	O21-Sm2-O20[4]	121.3(3)
O21-Sm2-O19[4]	76.0(3)	O21-Sm2-O28[2]	76.6(2)
O21-Sm2-O29[2]	73.7(3)	O21-Sm2-O12[3]	128.0(3)
O21-Sm2-O7	89.5(3)	O12[3]-Sm2-O13[3]	50.6(2)
O12[3]-Sm2-O20[4]	77.0(3)	O12[3]-Sm2-O19[4]	83.9(3)
O12[3]-Sm2-O28[2]	142.0(3)	O12[3]-Sm2-O29[2]	152.8(3)
O7-Sm2-O13[3]	72.9(3)	O7-Sm2-O20[4]	148.9(3)
O7-Sm2-O19[4]	144.8(3)	O7-Sm2-O28[2]	70.7(3)
O7-Sm2-O29[2]	119.8(3)	O7-Sm2-O12[3]	80.2(3)
O4-Na2-O4[5]	158.7(4)	O4-Na2-O15[3]	116.3(2)
O4[5]-Na2-O15[3]	69.8(2)	O4-Na2-O15[1]	69.8(2)
O4[5]-Na2-O15[1]	116.3(2)	O4-Na2-O5	53.0(2)
O4[5]-Na2-O5[5]	53.0(2)	O4[5]-Na2-O5	144.7(3)
O4-Na2-O5[5]	144.7(3)	O4-Na2-O27[3]	88.0(2)
O4[5]-Na2-O27[3]	75.5(2)	O4[5]-Na2-O27[1]	88.0(2)
O4-Na2-O27[1]	75.5(2)	O15[3]-Na2-O15[1]	149.3(4)
O5[5]-Na2-O15[1]	78.7(2)	O5-Na2-O15[1]	83.6(2)
O5-Na2-O15[3]	78.7(2)	O5[5]-Na2-O15[3]	83.6(2)
O5-Na2-O5[5]	109.1(4)	O27[1]-Na2-O15[1]	67.1(2)
O27[1]-Na2-O15[3]	142.9(3)	O27[3]-Na2-O15[1]	142.9(3)
O27[3]-Na2-O15[3]	67.1(2)	O27[1]-Na2-O5	127.3(2)
O27[1]-Na2-O5[5]	106.8(2)	O27[3]-Na2-O5	106.8(2)
O27[3]-Na2-O5[5]	127.3(2)	O27[1]-Na2-O27[3]	79.0(4)
O5-Na1-O13[3]	98.4(3)	O5-Na1-O8[5]	81.3(3)
O5-Na1-O8	87.2(3)	O5-Na1-O11	107.1(3)
O5-Na1-O1W	173.8(4)	O8[5]-Na1-O13[3]	172.7(3)
O8-Na1-O13[3]	106.1(3)	O8-Na1-O8[5]	81.3(3)
O8-Na1-O11	151.5(3)	O8-Na1-O1W	87.3(3)
O11-Na1-O13[3]	96.2(3)	O11-Na1-O8[5]	76.9(3)
O1W-Na1-O13[3]	80.2(3)	O1W-Na1-O8[5]	100.8(3)
O1W-Na1-O11	79.1(4)		

[1]1-X,1-Y,1-Z; [2]1-X,+Y,1/2-Z; [3]+X,1-Y,1/2+Z; [4]1/2-X,1/2-Y,1-Z; [5]1-X,+Y,3/2-Z; [6]+X,1-Y,-1/2+Z

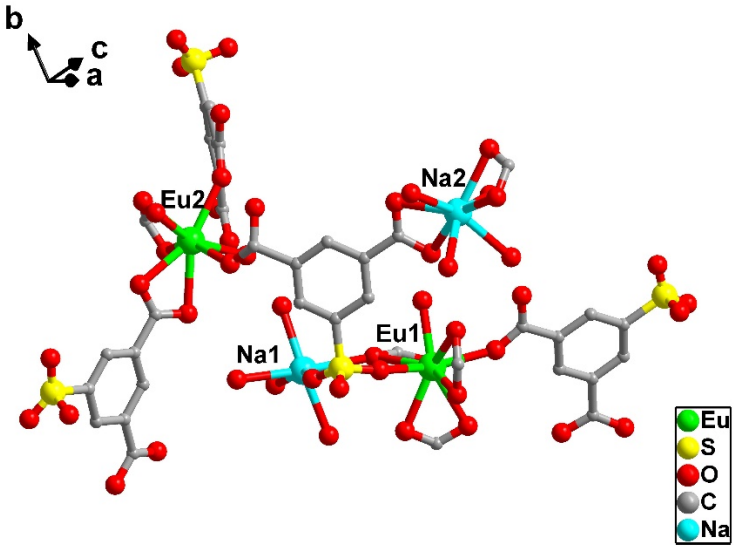

Fig. S1. The asymmetric unit of **FUT-2-Eu**.

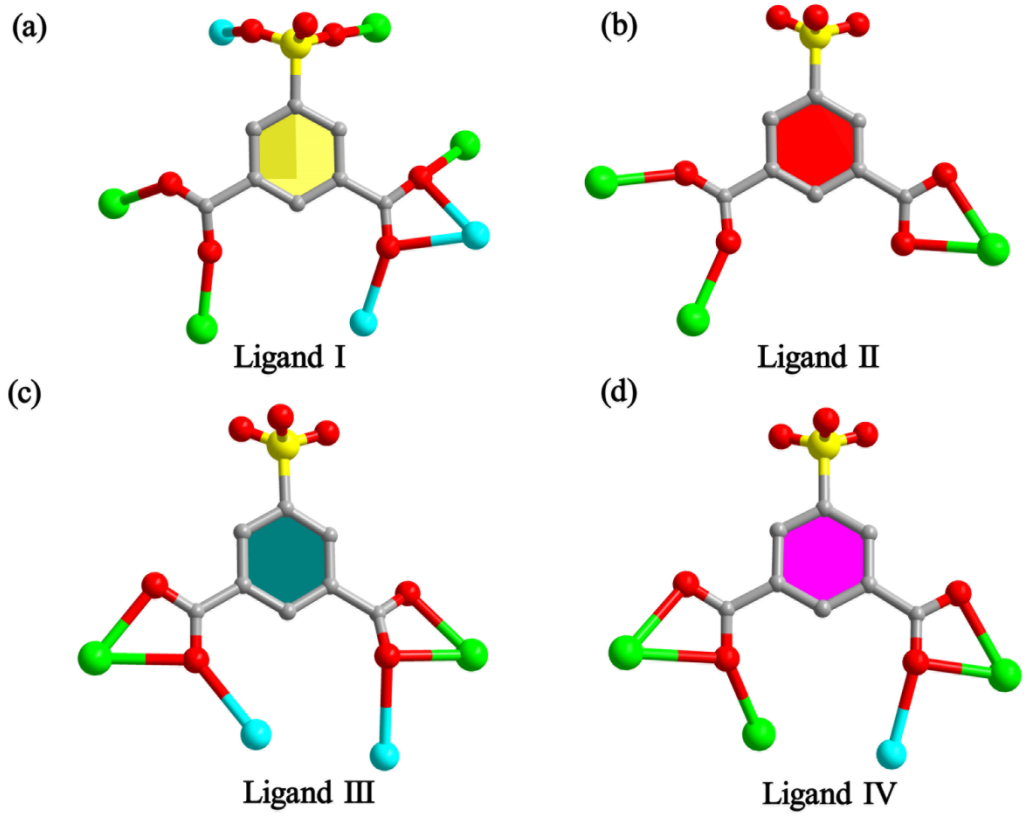

Fig. S2. Four crystallographic independent SIP^{3-} ligands exhibit three different coordination modes in **FUT-2-Eu**.

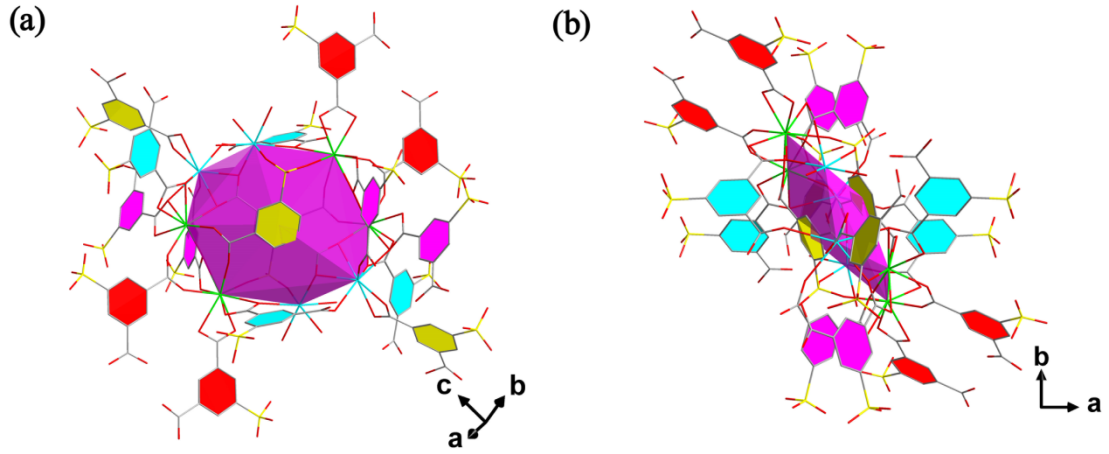

Fig. S3. Perspective views of the coordination environments of the metalloring cluster organic cage in **FUT-2-Eu**.

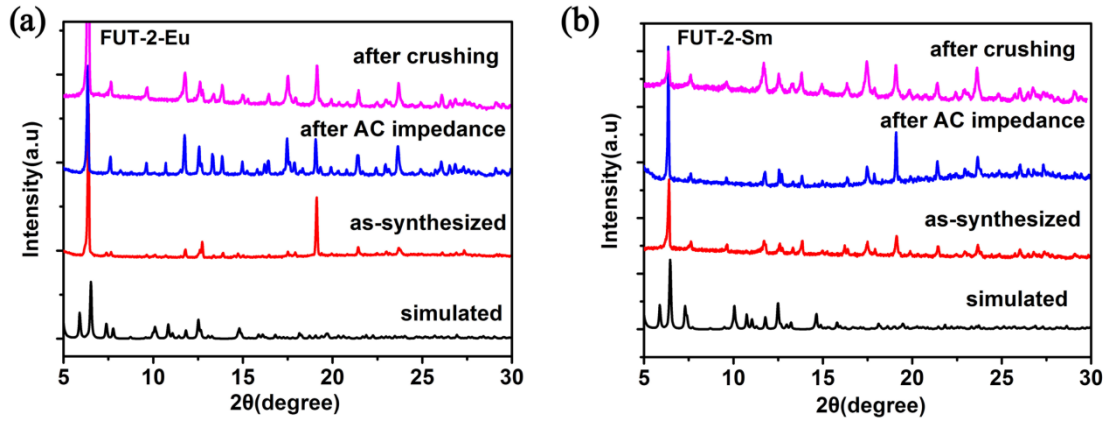

Fig. S4. Powder X-ray diffraction patterns of simulated, as-synthesized, after AC impedance measurements and after crushing of **FUT-2-Eu** (a) and **FUT-2-Sm** (b), indicate its purity as well as stability under after AC impedance measurements.

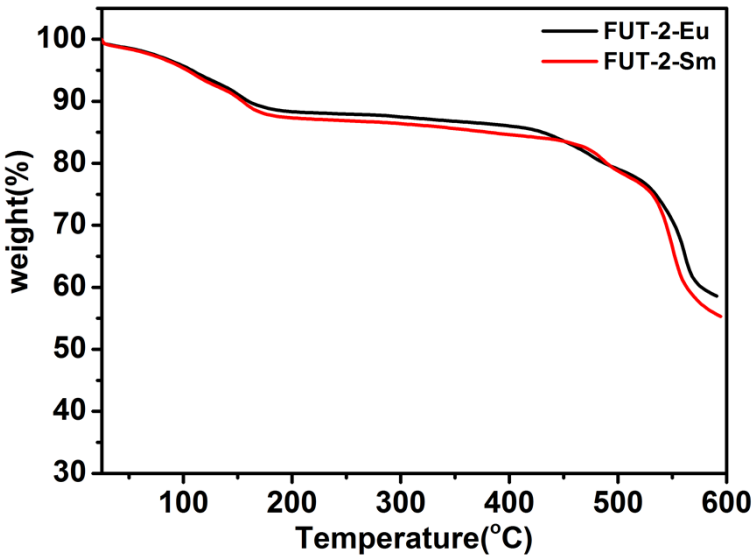

Fig. S5. TGA curves of **FUT-2-Eu** and **FUT-2-Sm**. The results suggest that almost all of the guest molecules were removed below ~234 °C, and no further weight loss was observed until 430 and 465 °C, respectively.

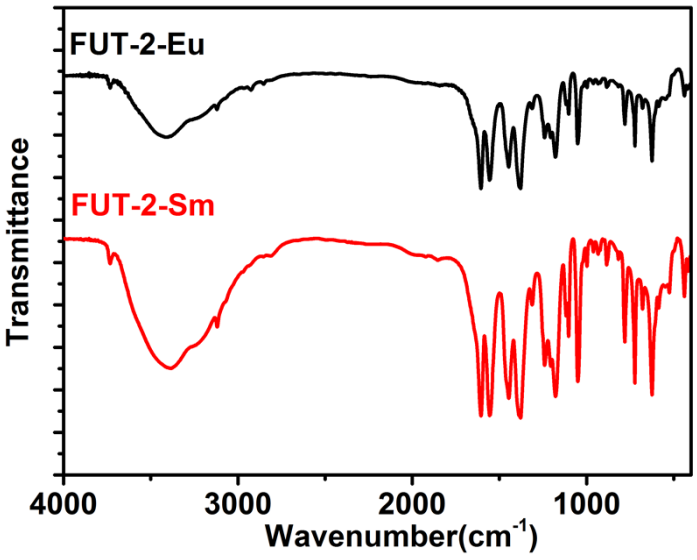

Fig. S6. IR spectra of **FUT-2-Eu** and **FUT-2-Sm**.

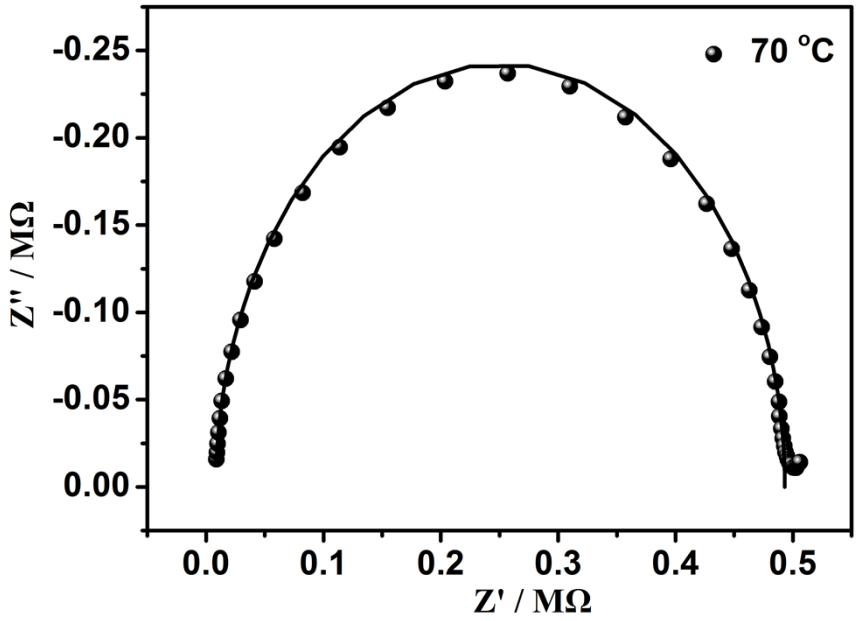

Fig. S7 Nyquist plots of **FUT-2-Sm** at 70 °C under non-humidified conditions (scatters represent experimental data, and lines do fitting data from equivalent circuits).

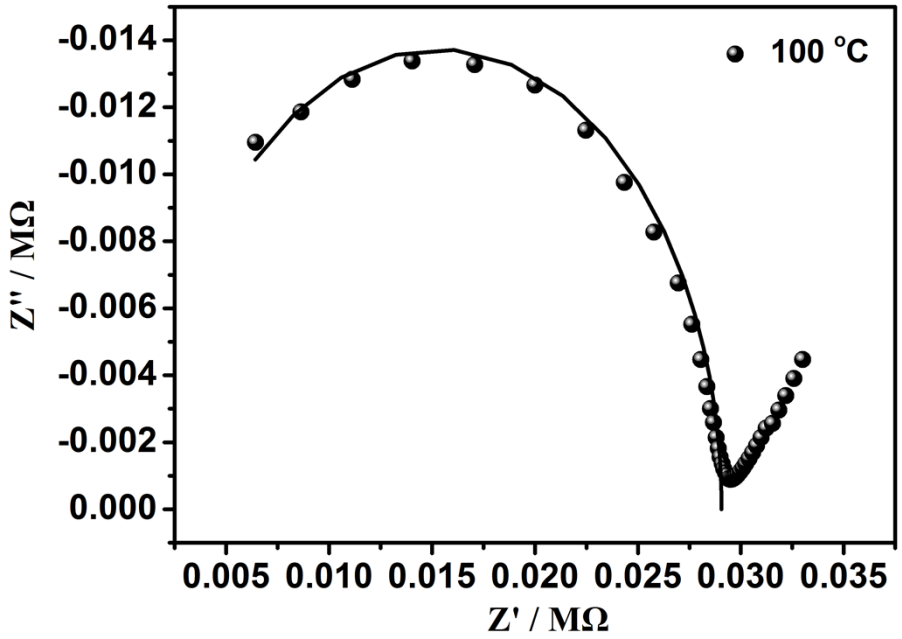

Fig. S8 Nyquist plots of **FUT-2-Eu** at 100 °C under non-humidified conditions (scatters represent experimental data, and lines do fitting data from equivalent circuits).

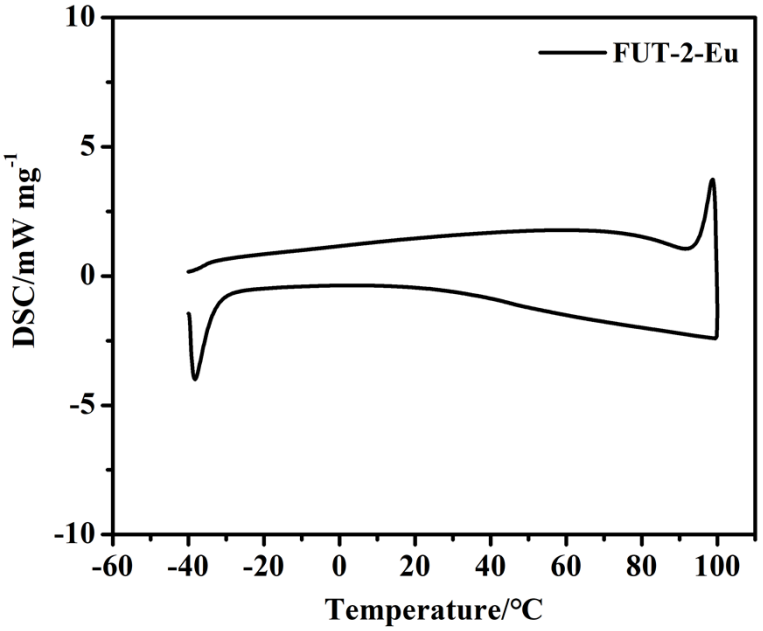

Fig. S9 DSC curve of **FUT-2-Eu**. The measurement was range from -40 to 100 °C, which doesn't present a clear peak, suggesting that no phase transition occurred in the framework.

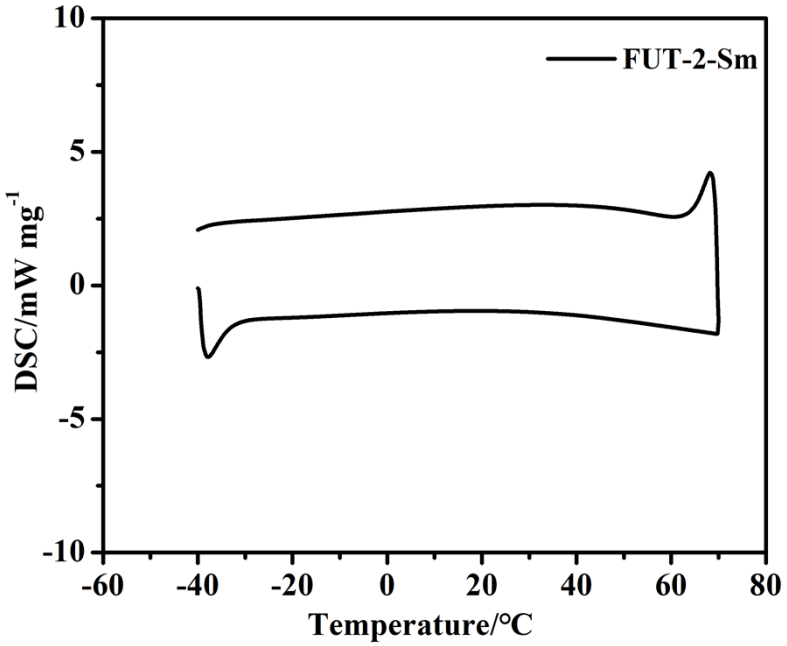

Fig. S10 DSC curve of **FUT-2-Sm**. The measurement was range from -40 to 70 °C, which doesn't present a clear peak, suggesting that no phase transition occurred in the framework.

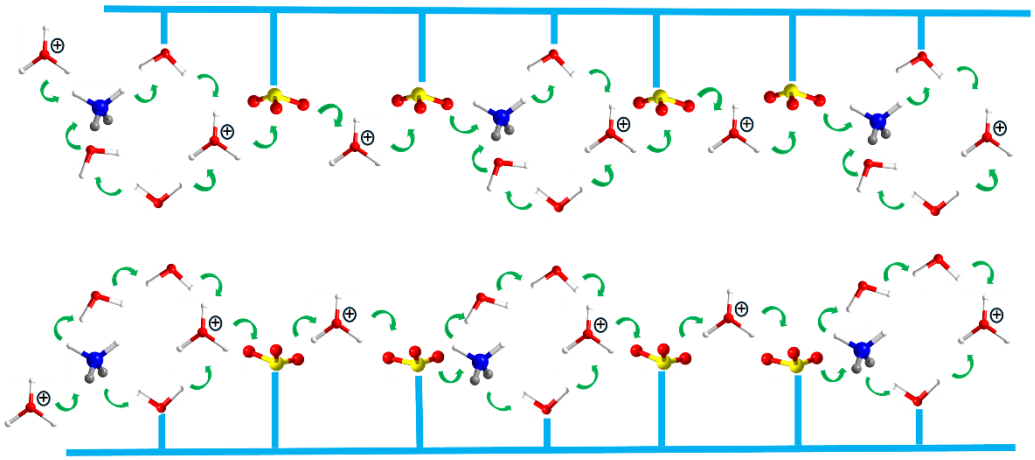

Fig. S11 View of the possible proton transport in the **FUT-2-Eu**.

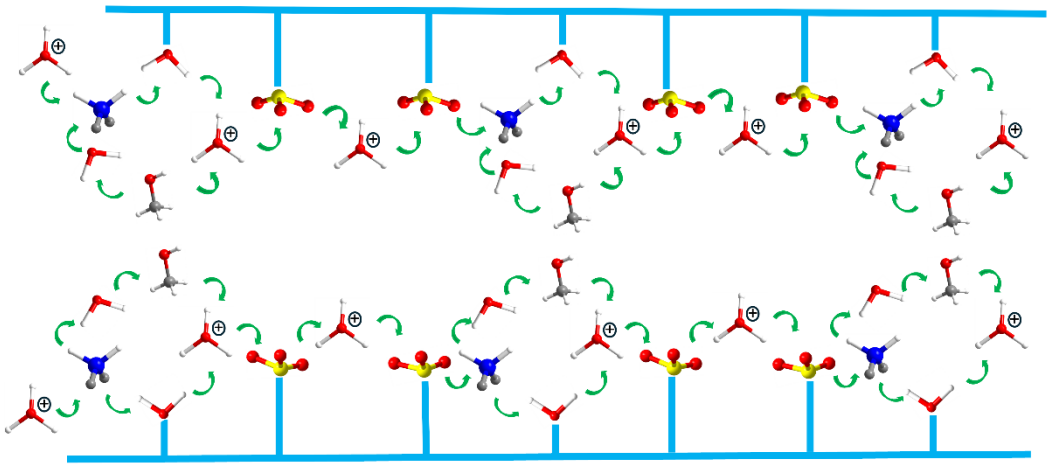

Fig. S12 View of the possible proton transport in the **FUT-2-Sm**.

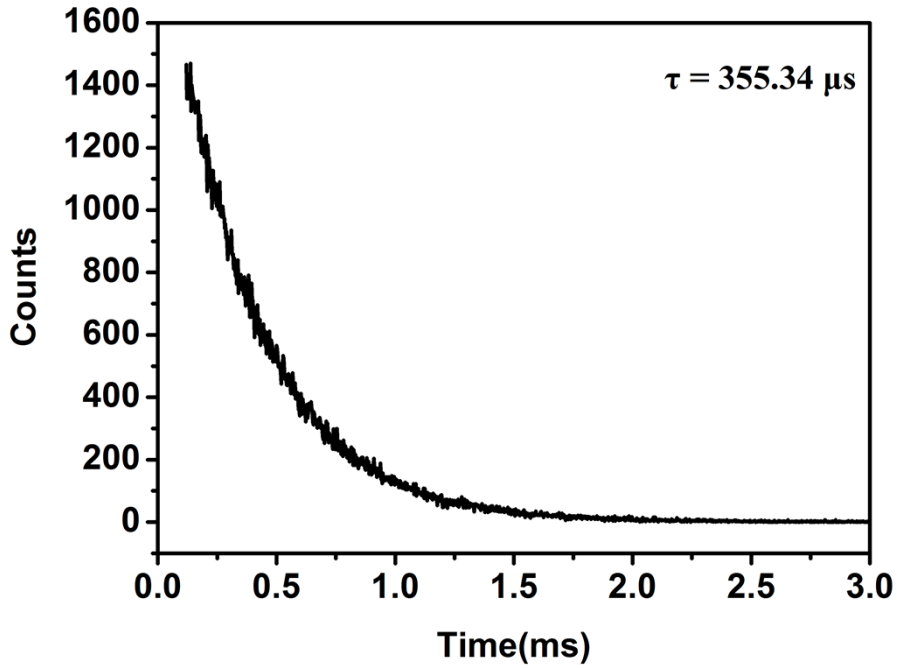

Fig. S13. Fluorescence decay curves of **FUT-2-Eu** measured at room temperature.

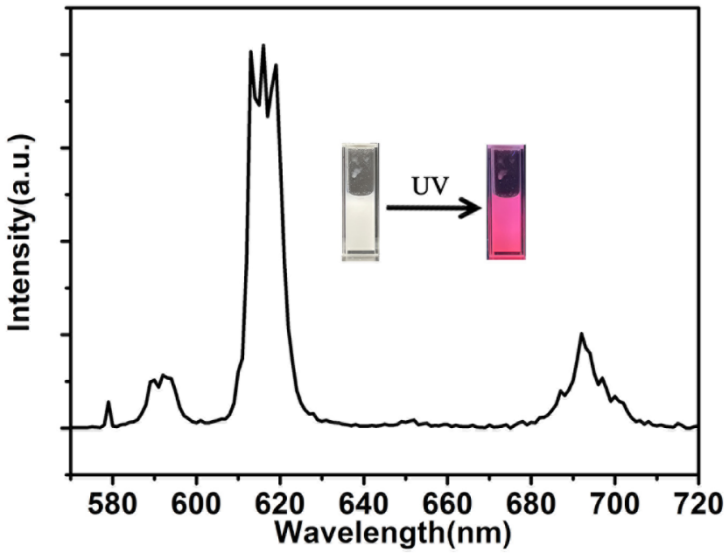

Fig. S14. The luminescence spectra of **FUT-2-Eu** in DMA solution. The inset shows the corresponding picture before and after 365 nm ultraviolet light irradiation.

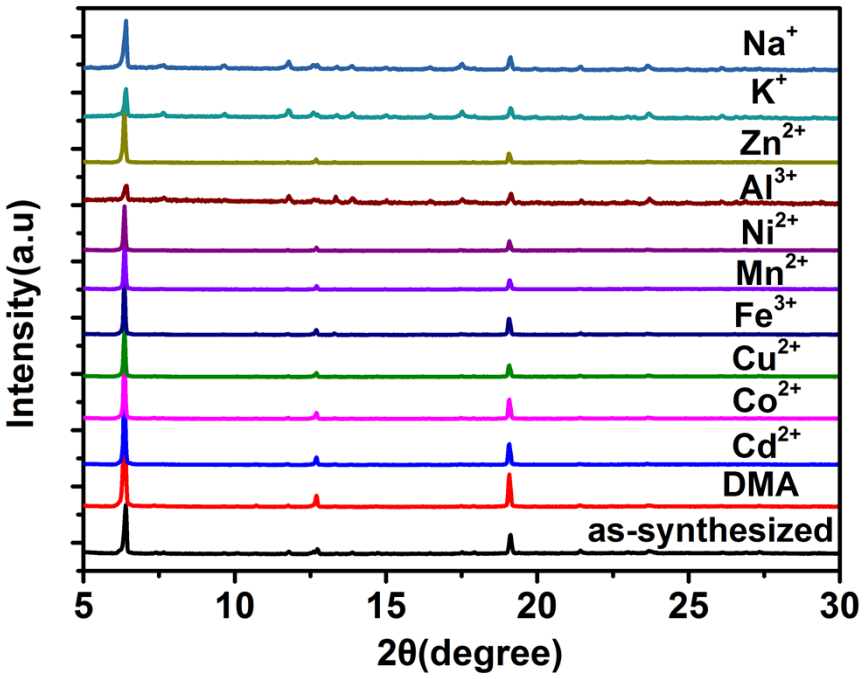

Fig. S15. The powder X-ray diffraction patterns of **FUT-2-Eu** after immersing in DMA solution containing 1mM of several metal ions for 12 hours.

Fig. S16. The Photos of **FUT-2-Eu** soaked in Fe^{3+} solution and washed with DMA solution.

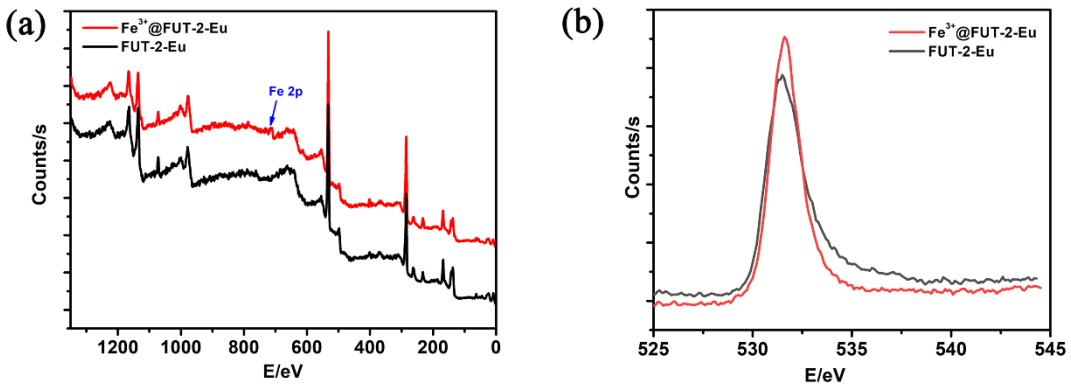

Fig. S17. (a) XPS spectra for **Fe^{3+}@FUT-2-Eu** and **FUT-2-Eu**. (b) XPS spectra of O1s for **Fe^{3+}@FUT-2-Eu** and **FUT-2-Eu**.

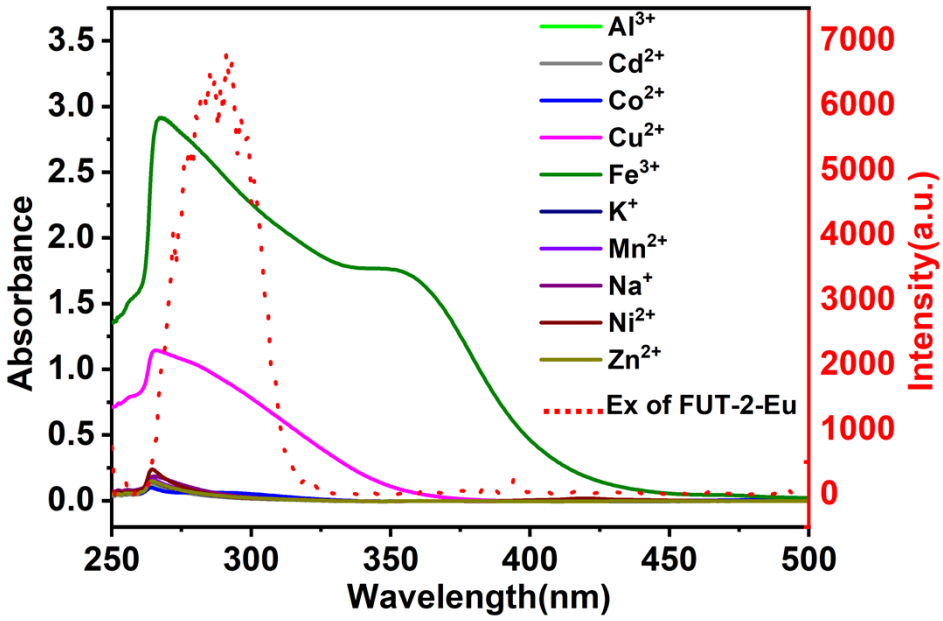

Fig. S18. Solid line: UV-Vis spectra of DMA solutions containing 10^{-3} M $M(NO_3)_x$ (M = Al^{3+}, Cd^{2+}, Co^{2+}, Cu^{2+}, Fe^{3+}, K^+, Mn^{2+}, Na^+, Ni^{2+}, Zn^{2+}); Dotted line: Excitation spectra of dispersed 10 mg **FUT-2-Eu** in 5mL DMA solutions.

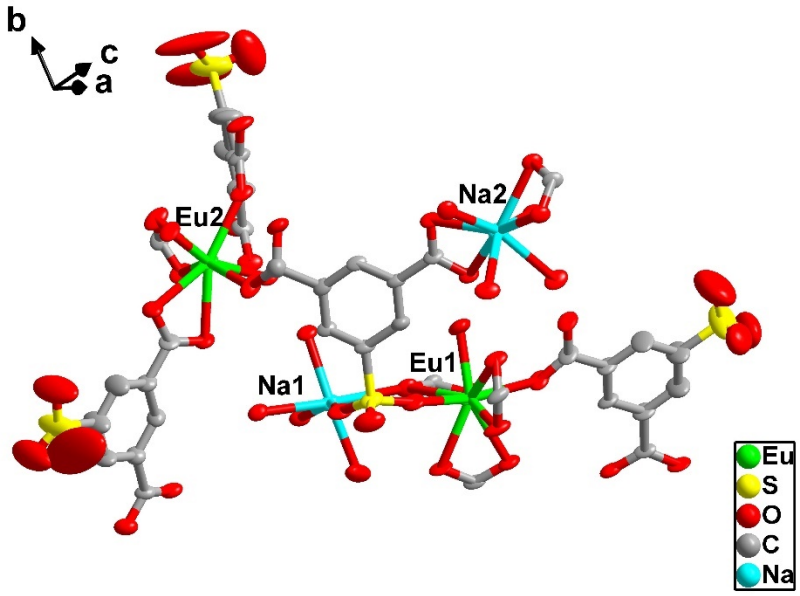

Fig. S19. The ellipsoid plot of **FUT-2-Eu**.

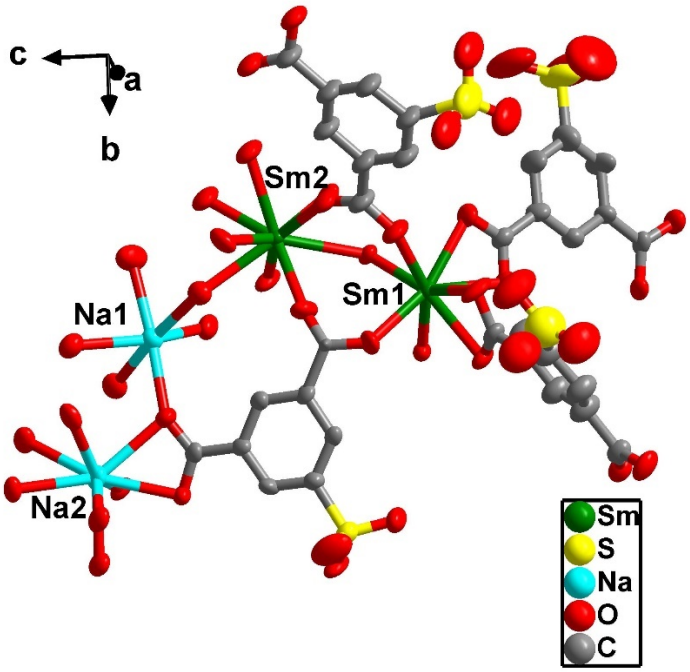

Fig. S20. The ellipsoid plot of **FUT-2-Sm**.

Table S4 Compare the proton conductivity of **FUT-2-Eu** with that of other sulfonic acid-carboxylate MOFs.

Compounds	Proton Conductivity (S cm^{-1})	conditions	Working Temperature Range (°C)	Ref
FUT-2-Eu	2.65×10^{-3}	90 °C	-40~90	**This work**
YCu161	1.84×10^{-3}	90 °C and 98%RH	30~90	S9
Zr-$(NDC)_{0.3}(SNDC)_{0.7}$	3.18×10^{-4}	90 °C and 98% RH	30~90	S10
BUT-77	3.08×10^{-2}	80 °C and 100% RH	25~80	S11
$(Me_2NH_2)_2(H_3O)[GdL_2]\cdot8H_2O$	8.83×10^{-3}	95 °C and 60%RH	25~95	S12
VNU-17	6.65×10^{-6}	70 °C and 98%RH	30~70	S13
$Co(dia)_{1.5}(Hsip)(H_2O)\cdot H_2O$	3.461×10^{-5}	85 °C and98%RH	40~85	S14
JXNU-7	1.04×10^{-4}	85 °C and98%RH	45~85	S15
CUST-736a	2.25×10^{-3}	80 °C and98%RH	50~80	S16
VNU-23	1.54×10^{-4}	70 °C and90%RH	30~70	S17
$[Cu(H_2L)(DMF)_4]_n$	3.46×10^{-3}	95 °C and 95% RH	25~95	S18
$Cu_4(L)_2(OH)_2(DMF)_2$	7.4×10^{-3}	95 °C and 95%RH	35~95	S19
Cu-DSOA	1.9×10^{-3}	85 °C and 98%RH	25~100	S20
Tb-DSOA	1.66×10^{-4}	100 °C and 98%RH	40~100	S21
$\{(H_3O)[Eu(SBDB)(H_2O)_2]\}_n$	1.0×10^{-4}	65 °C and 98% RH	17~65	S22
Ni-MOF	1.95×10^{-3}	85 °C and 95% RH	30~85	S23
PCMOF-17	1.17×10^{-3}	25 °C and 40% RH	25~50	S24
UiO-66-SO_3H	0.34×10^{-2}	30 °C and 97% RH	18~30	S25
BUT-8(Cr)	4.63×10^{-2}	80 °C and 100% RH	25~80	S26
MIL-101-SO_3H	1.16×10^{-2}	80 °C and 100% RH	25~80	S26

Table S5 Comparison of the detection limits and K_{sv} values for Fe^{3+} of the selected Ln-MOF.

Ln-MOF	K_{SV} M^{-1}	detection limit/μM	ref
534-MOF-Tb	5.51×10^3	130	S27
FJU-13-Eu	2.03×10^4	1.41	S28
1-Eu	4.75×10^4	6.32	S29
{[Tb(L)(DMA)]·(DMA)·($0.5H_2O$)}	1.91×10^3	-	S30
$[Tb(tftba)_{1.5}(phen)(H_2O)]_n$	4.04×10^4	12.7	S31
La-TCPE	1.09×10^5	1.69	S32
$\{[Eu(L)\ (BPDC)_{1/2}(NO_3)]\cdot H_3O\}_n$	5.16×10^4	-	S33
$[[Eu_2(pdba)_3(H_2O)_3]\cdot 2H_2O]_n$	6.53×10^3	-	S34
$[[Eu(bpda)_{1.5}]\cdot H_2O]_n$	1.25×10^4	0.9	S35
$[Sm(L)_2(OH)(H_2O)_3]_n$	1.03×10^4	3.21	S36
FUT-2-Eu	1.66×10^4	3.64	**This work**

Supplementary references

(1) A. V. Dolomanov, L. J. Bourhis, R. J. Gildea, J. A. K. Howard, and H. Puschmann, OLEX2: a complete structure solution, refinement and analysis program, *J. Appl. Crystallogr.,* 2009, **42**, 339–341.

(2) L. Palatinus, and G. Chapuis, SUPERFLIP - a computer program for the solution of crystal structures by charge flipping in arbitrary dimensions, *J. Appl. Crystallogr*., 2007, **40**, 786-790.

(3) G. M. Sheldrick, A short history of SHELX, *Acta Crystallogr. Sect. A,* 2008, **64**, 112-122.

(4) L. Sarkisov, and A. Harrison, Computational structure characterisation tools in application to ordered and disordered porous materials, *Mol. Simul*., 2011, **37**, 1248-1257.

(5) A. L. Spek, Single-crystal structure validation with the program PLATON, *J. Appl. Crystallogr*., 2003, **36**, 7-13.

(6) Y. Ye, L. Zhang, Q. Peng, G. Wang, Y. Shen, Z. Li, L. Wang, X. Ma, Q. H. Chen, Z. Zhang, and S. Xiang, High Anhydrous Proton Conductivity of Imidazole-Loaded Mesoporous Polyimides over a Wide Range from Subzero to Moderate Temperature, *J. Am. Chem. Soc*., 2015, **137**, 913–918.

(7)X. L. Su, Z. Z. Yao, Y. X. Ye, H. Zeng, G. Xu, L. Wu, X. L. Ma, Q. H. Chen, L. H. Wang, Z. J. Zhang, and S. C. Xiang, 40-Fold Enhanced Intrinsic Proton Conductivity in Coordination Polymers with the Same Proton-Conducting Pathway by Tuning Metal Cation Nodes, *Inorg. Chem*., 2016, **55**, 983−986.

(8) A. K. Rappe, C. J. Casewit, K. S. Colwell, W. A. Goddard, W. M. Skiff, UFF, a Full Periodic-Table Force-Field for Molecular Mechanics and Molecular-Dynamics Simulations. *J. Am. Chem. Soc.* **1992**, *114*, 10024-10035.

(9) L. Zhao, R. Zhu, S. Wang, L. He, L. Du, and Q. Zhao, Multiple Strategies to Fabricate a Highly Stable 2D CuIICuI−Organic Framework with High Proton Conductivity, *Inorg. Chem*., 2021, **60**, 16474-16483.

(10) J. Zheng, Q. Wang, F. Jiang, Y. Li, X. Huang, X. Sun, W. Dong, D. Ba, J. Zhao, D. Li. Enhanced proton conductivity by incorporating sulfonic acid groups into a zirconium-based metal-organic framework via ligand exchange, *Journal of Solid State Chemistry,* 2023, **324**,124070.

(11) G. Si, F. Yang, T. He, X. Kong, W. Wu, T. Li, K. Wang, and J. Li. Enhancing proton conductivity in Zr-MOFs through tuning metal cluster connectivity, *J. Mater. Chem. A,* 2022, **10**, 1236-1240.

(12) S. Zhang, Y. Xie, M. Yang, and D. Zhu, Porosity regulation of metal–organic frameworks for high proton conductivity by rational ligand design: mono- versus disulfonyl-4,4’-biphenyldicarboxylic acid, *Inorg. Chem. Front*., 2022, **9**, 1134.

(13) T. H. N. Lo, M. V. Nguyen, and T. N. Tu, Anchoring Strategy Leads to Enhanced Proton Conductivity in a New Metal-Organic Framework, *Inorg. Chem. Front*., 2017, **4**, 1509-1516.

(14) T. Ho, A. Datta, and H. M. Lee, Proton-conducting metal–organic frameworks with linkers containing anthracenyl and sulfonate groups, *CrystEngComm*., 2022, **24**, 5450.

(15) M. Xu, Y. Wang, Q. Liu, Z. Lin, and Q. Liu. Lanthanide 5,7-Disulfonate-1,4-naphthalenedicarboxylate Frameworks Constructed from Trinuclear and Tetranuclear Lanthanide Carboxylate Clusters: Proton Conduction and Selective Fluorescent Sensing of Fe^{3+}, *Inorg. Chem*., 2020, **59**, 7265-7273.

(16) Z. Feng, J. Li, J. Sun, X. Wu, Y. Li, D. Wu, S. Li, Wang, X. and Su, Z. Enhanced proton conductivity by guest molecule exchange in an acylamide-functionalized metal–organic framework, *Dalton Trans*., 2023, **52**, 6847–6852.

(17) M. V. Nguyen, T. H. N. Lo, L. C. Luu, H. T. T. Nguyena, and T. N. Tu, Enhancing Proton Conductivity in a Metal-Organic Framework at T > 80°C by Anchoring Strategy. *J. Mater. Chem. A*, 2018, **6**, 1816-1821.

(18) S. Zhao, X. Song, M. Zhu, X. Meng, L. Wu, S. Song, C. Wang, and H. Zhang, Assembly of Three Coordination Polymers Based on a Sulfoniccarboxylic Ligand Showing High Proton Conductivity, *Dalton Trans*., 2015, **44**, 948-954.

(19) X. Meng, S. Song, X. Song, M. Zhu, S. Zhao, L. Wu, and H. Zhang, A tetranuclear copper cluster-based MOF with sulfonate–carboxylate ligands exhibiting high proton conduction

properties, *Chem. Commun*., 2015, **51**, 8150-8152.
(20) X. Dong, R. Wang, J. Li, S. Zang, H. Hou, and T. C. W. Mak, A tetranuclear $Cu_4(\mu_3\text{-}OH)_2$-based metal–organic framework (MOF) with sulfonate–carboxylate ligands for proton conduction, *Chem. Commun*., 2013, **49**, 10590-10592.
(21) X. Dong, R. Wang, J. Wang, S. Zang, and T. C. W. Mak, Highly selective sensing Fe^{3+} and proton conduction in a water-stable sulfonate-carboxylate Tb-organic-framework, J. *Mater. Chem. A,* 2015, **3**, 641-647.
(22) Y. Yuan, S. Yang, C. Zhang, and Q. Wang, A new europium metal–organic framework with both high proton conductivity and highly sensitive detection of ascorbic acid, *CrystEngComm*., 2018, **20**, 6989–6994.
(23) S. Saha, M. Das, K. S. Das, R. Datta, S. Bala, J. Liu, P. P. Ray, and R. Mondal, Magnetic and Electric Properties of Pyrazole-Based Metal−Organic Frameworks Grafted With a Sulfonic Moiety, *Cryst. Growth Des.,* 2023, **23**, 1104−1118.
(24) B. Joarder, J. Lin, Z. Romero, and G. K. H. Shimizu, Single Crystal Proton Conduction Study of a Metal Organic Framework of Modest Water Stability, *J. Am. Chem. Soc*., 2017, **139**, 7176−7179
(25) F. Yang, H. Huang, X. Wang, F. Li, Y. Gong, C. Zhong, and J. Li, Proton Conductivities in Functionalized UiO-66: Tuned Properties, Thermogravimetry Mass, and Molecular Simulation Analyses, *Cryst. Growth Des.,* 2015, **15**, 5827−5833.
(26) F. Yang, G. Xu, Y. Dou, B. Wang, H. Zhang, H. Wu, W. Zhou, J. Li, and B. Chen, A flexible metal–organic framework with a high density of sulfonic acid sites for proton conduction, *Nature Energy*, 2017, **2**, 877-883.
(27) M. Chen, W. M. Xu, J. Y. Tian, H. Cui, J. X. Zhang, C. S. Liu, and M. Du, A terbium (III) lanthanide–organic framework as a platform for a recyclable multi-responsive luminescent sensor, *J. Mater. Chem. C,* 2017, ***5***, 2015-2021.
(28) L. Liu, Y. Wang, R. Lin, Z. Yao, Q. Lin, L. Wang, Z. Zhang, and S. Xiang, Two water-stable lanthanide metal–organic frameworks with oxygen-rich channels for fluorescence sensing of Fe(III) ions in aqueous solution, *Dalton Trans*., 2018, **47**, 16190-16196.
(29) H. Chen, L. Fan, H. Lv, and X. Zhang, Robust Anionic Ln^{III}–Organic Frameworks: Chemical Fixation of CO_2, Tunable Light Emission, and Fluorescence Recognition of Fe^{3+}, *Inorg. Chem*., 2020, **59**, 13407-13415.
(30) S. Pal, and P. K. Bharadwaj, A luminescent terbium MOF containing hydroxyl groups exhibits selective sensing of nitroaromatic compounds and Fe (III) ions, *Cryst. Growth Des.*, 2016, **16** , 5852.
(31) H. H. Yu, J. Q. Chi, Z. M. Su, X. Li, J. Sun, C. Zhou, X. L. Hu, and Q. Liu, A water-stable terbium metal–organic framework with functionalized ligands for the detection of Fe^{3+} and $Cr_2O_7^{2-}$ ions in water and picric acid in seawater, *CrystEngComm.*, 2020, **22**, 3638–3643.
(32) L. Yang, Y. Dou, L. Qin, L. Chen, M. Xu, C. Kong, D. Zhang, Z. Zhou, and S. Wang, A Lanthanide-Containing Coordination Polymer Using Tetraphenylethene-Based Linkers with Selective Fe^{3+} Sensing and Efficient Iodine Adsorption Activities, *Inorg. Chem*., 2020, **59**, 16644−16653.
(33) W. Yan, C. Zhang, S. Chen, L. Han, and H. Zheng, Two Lanthanide Metal−Organic Frameworks as Remarkably Selective and Sensitive Bifunctional Luminescence Sensor for Metal Ions and Small Organic Molecules, *ACS Appl. Mater. Interfaces,* 2017, **9**, 1629−1634.
(34) H. Li, Y. Han, Z. Shao, N. Li, C. Huang, and H. Hou, Water-stable Eu-MOF fluorescent sensors for trivalent metal ions and nitrobenzene, *Dalton Trans*., 2017, **46**, 12201–12208.
(35) J. Wang, J. Wang, Y. Li, M. Jiang, L. Zhang, and P. Wu, A europium (III)-based metal–organic framework as a naked-eye and fast response luminescence sensor for acetone and ferric iron. *New J. Chem.*, 2016, **40**, 8600–8606.
(36) Z. Xie, T. Yue, Q. Dong, Q. Ma, Q. Cao, L. Wang, D. Wang, Selective detection of Fe^{3+} and Congo red adsorption properties studies of Ln-complexes based on imidazopyridine carboxylic acid ligand, *Polyhedron*, 2024, **249**, 116777.